THE JOURNAL OF PHYSICAL CHEMISTRY A

Article

pubs.acs.org/JPCA

Liquid–Liquid Phase Separation in Mixed Organic/Inorganic Single Aqueous Aerosol Droplets

D. J. Stewart,[†] C. Cai,[†,‡] J. Nayler,[†] T. C. Preston,[†] J. P. Reid,*[,†] U. K. Krieger,[§] C. Marcolli,[§,∥] and Y. H. Zhang[‡]

[†]School of Chemistry, University of Bristol, Bristol BS8 1TS, U.K.

[‡]The Institute of Chemical Physics, Key Laboratory of Cluster Science, Beijing Institute of Technology, Beijing 100081, People's Republic of China

[§]Institute for Atmospheric and Climate Science, ETH Zurich, Zurich, Switzerland

[∥]Marcolli Chemistry and Physics Consulting GmbH, Zurich, Switzerland

ABSTRACT: Direct measurements of the phase separation relative humidity (RH) and morphology of aerosol particles consisting of liquid organic and aqueous inorganic domains are presented. Single droplets of mixed phase composition are captured in a gradient force optical trap, and the evolving size, refractive index (RI), and morphology are characterized by cavity-enhanced Raman spectroscopy. Starting at a RH above the phase separation RH, the trapped particle is dried to lower RH and the transition to a phase-separated structure is inferred from distinct changes in the spectroscopic fingerprint. In particular, the phase separation RHs of droplets composed of aqueous solutions of polyethylene glycol (PEG-400)/ammonium sulfate and a mixture of C6-diacids/ammonium sulfate are probed, inferring the RH from the RI of the droplet immediately prior to phase separation. The observed phase separation RHs occur at RH marginally higher (at most 4%) than reported in previous measurements made from studies of particles deposited on hydrophobic surfaces by brightfield imaging. Clear evidence for the formation of phase-separated droplets of core–shell morphology is observed, although partially engulfed structures can also be inferred to form. Transitions between the different spectroscopic signatures of phase separation suggest that fluctuations in morphology can occur. For droplets that are repeatedly cycled through the phase separation RH, the water activity at phase separation is found to be remarkably reproducible (within ±0.0013) and is the same for the 1-phase to 2-phase transition and the 2-phase to 1-phase transition. By contrast, larger variation between the water activities at phase separation is observed for different droplets (typically ±0.02).

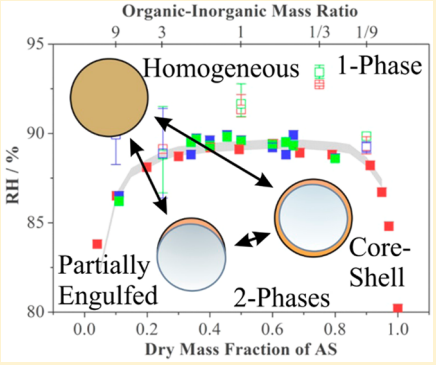

I. INTRODUCTION

Aerosol particles are an important atmospheric constituent, influencing atmospheric chemistry,[1,2] air quality, and global climate.[3−7] Their impact is highly dependent on their properties, including particle size, phase, and morphology.[3,8,9] However, the dependence of these properties on particle composition and environmental conditions, specifically relative humidity (RH) and temperature, remains poorly understood, leading to uncertainties in the magnitudes of the impacts of aerosols on climate and chemistry. Tropospheric aerosol is complex in composition containing organic matter (both primary and secondary with a large range of O:C ratios), inorganic salts (mainly ammonium, sulfate, and nitrate in the accumulation mode particle size range[10]), and water. These components can be internally mixed and, depending on the composition of the aerosol and the ambient conditions, may be one liquid phase, two liquid phases, an amorphous glassy state, a solid crystalline state, or indeed a mixture of these states.[11]

The phase of an aerosol particle is dependent on the immediate history of exposure to changing temperature and RH.[11] As ambient conditions change, an aerosol particle may go through some or all of the possible phases in a relatively short time; the time scale is dependent on the equilibration time for gas–particle partitioning of water and other components. Time scales for equilibration can be of the order of seconds to minutes for high-volatility components in liquid particles to hours or days for components of lower-volatility in solid or glassy aerosol.[12,13] An understanding of the conditions and time scales under which phase transitions occur is needed if our understanding of the behavior of aerosols in the atmosphere is to be developed. The deliquescence and efflorescence phase behavior of atmospheric aerosol is relatively well-understood,[14−21] and there is an increasing awareness and understanding of the behavior of "glassy" aerosol[22−25] and the conditions under which it is formed. Until recently, however, there has been little consideration of the phase separation of a

Received: February 18, 2015
Revised: April 8, 2015
Published: April 16, 2015

DOI: 10.1021/acs.jpca.5b01658
J. Phys. Chem. A 2015, 119, 4177−4190

homogeneous liquid particle into two liquid phases consisting of a predominantly hydrophilic domain containing inorganic solutes and a hydrophobic domain containing water insoluble organic components.

Studies of liquid−liquid phase separation (LLPS) in mixed organic/inorganic particles are relatively sparse, but some broad conclusions can be drawn from the available data. Laboratory measurements on complex organic/ammonium sulfate (AS) mixtures with up to 10 organic components[15,26,27] have shown that LLPS *always* occurs if the O:C ratio is <0.56. In the intermediate range, 0.56 < O:C < 0.8, the occurrence of LLPS is dependent on the specific functional groups forming the organic component[15,26] and the organic-to-sulfate mass ratio.[14] Recently, Song et al.[28] extended the range of O:C ratio covered to 0.29−1.33 and reported data for particles of 33 different organic compositions (all with AS as the inorganic salt component) with the organic fraction composed of between 1 and 10 components. In most mixtures with O:C from 0.29 to 0.60, LLPS occurred over the whole range of organic-to-inorganic mass ratio (OIR) while systems with an O:C in the 0.80−1.33 range exhibited no LLPS. Systems with O:C ratios in the intermediate range (O:C of 0.6−0.8) once again showed LLPS over a range of OIR that depended upon the composition of the organic fraction. The phase separation RH (SRH) observed for these particles varied from 59.0 to 100% RH with no clear relationship to the O:C ratio and OIR mass ratio. You et al. explored LLPS for ammonium bisulfate, ammonium nitrate and sodium chloride salts in mixtures with 23 different organic species, extending the observations of LLPS beyond measurements with AS as the inorganic salt. Consistent with mixtures containing AS, LLPS was never observed for O:C ≥ 0.8 and always observed for O:C < 0.5 for the 92 types of particles studied, regardless of the salt type.[29] Ambient aerosol samples collected on substrates have also been investigated. Aerosol collected in Atlanta,[30] heavily influenced by both anthropogenic and biogenic emissions with an O:C ratio of ∼0.5, showed LLPS. Aerosol sampled in the Amazon,[31] a region dominated by biogenic emissions, also exhibited LLPS over a range of O:C ratios consistent with the work of Song et al.[26]

The morphology adopted by particles containing immiscible liquid domains after phase separation remains poorly understood. The arrangement of the phases adopted may be core−shell or partially engulfed, or may even contain small domains of one phase dispersed throughout the second. Reid and co-workers have provided a framework for predicting the morphology of liquid−liquid phase-separated particles, with the formation of a core−shell or partially engulfed structure dependent on not only the surface and interfacial tensions of the hydrophilic and hydrophobic phase domains, but also the relative phase volumes.[32−35] The morphology of a particle affects a wide range of physical, chemical, and optical properties; thus, morphology can influence the effect of aerosols on the chemistry of the atmosphere and climate.[36] In atmospheric chemistry, the heterogeneous reactions of gas-phase species (such as ozone or N_2O_5) on the surface of aerosol particles play an important role in the removal of species that affect the oxidative balance of the atmosphere. The efficiency of these reactions in contributing to the removal of gas-phase species is likely dependent on the morphology of the particle and the chemical identity of the liquid phase exposed directly to the gas phase. For example, the hydrolysis of N_2O_5 on the surface of an aerosol will be inhibited by a partially engulfed particle as compared to a homogeneous aerosol particle because of the lower aqueous surface area. Indeed, if a core−shell morphology is adopted, then the reaction may be effectively suppressed if the droplet is coated in an organic shell.[37] Recent work has shown that the reaction can still occur when the particle adopts a core−shell morphology, albeit with a much reduced uptake coefficient.[38] Then, the exact decrease in reaction rate is determined by the hygroscopicity and viscosity of the organic shell. The morphology of a particle can also affect the hygroscopicity of the particle and the accessibility of sites for ice nucleation with the existence of an organic-rich lens or shell at the surface of a particle affecting the kinetics of gas−particle partitioning of water.[39,40]

Reid et al.[32] assessed the compositional dependence of the surface and interfacial tensions of the aqueous and organic phase volumes forming a particle for a large number of organic components, considering also the influence of the salting-out of organic components from the aqueous phase domain and the consequent influence on morphology. Their survey was limited to 65 organic components with an O:C ratio ranging from 0 to 0.6, with 90% having ratios less than 0.25 and only one compound with a ratio >0.5. For these systems, they concluded that partially engulfed structures should predominate. Bertram et al.[14] and Ciobanu et al.[41] concluded that core−shell morphologies are adopted for aerosol containing organic components with an O:C ratio <0.7 from measurements made on particles deposited on hydrophobic coverslips and using brightfield imaging microscopy. Notably, Bertram et al.[14] studied the phase behavior of mixed solutions with AS and 18 organic components, but with 15 components having O:C ratios of >0.5 and the lowest having an O:C ratio of 0.29. Ciobanu et al.[41] studied the ternary poly(ethylene glycol)-400/ammonium sulfate/water system alone with the organic component having an O:C ratio of 0.56. The potential influence of the substrate on the particle phase behavior and morphology is unclear, although assumed to be negligible. The Atlanta samples reported by You et al.[30] (O:C ∼ 0.5) also suggested core−shell morphology when LLPS was observed. Song et al.[28] considered 33 components with O:C ratios ranging from 0.29 to 1.33 and observed the formation of both partially engulfed and core−shell morphologies for mixtures of dicarboxylic acids (diacids) and AS. Indeed, for a mixture of C6 and C7 diacids with AS (OIR of 0.67), phase separation to a core−shell morphology was observed at a RH of 83.5% followed by a change to a partially engulfed structure as the RH was lowered below 80%. A similar transition in morphology was observed for droplets containing AS and a mixture of C6-diacids (OIR of 1:1 and 1:2), with the transition occurring at progressively lower RH as the OIR was reduced. For mixtures of C7 diacids and AS (OIR of 2:1) and C5/C6/C7 diacids and AS (OIR of 1:1), spinodal decomposition was observed and led directly to partially engulfed structures. A comparison of these studies suggests that phase-separated aerosols formed from hydrophobic and hydrophilic phase domains are likely to form partially engulfed structures if the organic components forming the hydrophobic phase are of low O:C ratio with an increasing trend toward core−shell with increasing O:C. However, the differences in energies between different morphologies are often only slight and switching between configurations may occur.[32]

Direct observations of liquid−liquid phase-separated particles in the aerosol phase rather than of sampled particles deposited on substrates have been limited. Measurements using aerosol

DOI: 10.1021/acs.jpca.5b01658
J. Phys. Chem. A 2015, 119, 4177−4190

optical tweezers have reported the direct formation of partially engulfed morphology structures on LLPS, albeit from studies with particles containing decane, octanol, or oleic acid with O:C <0.1, i.e., lower than that for the imaging microscopy studies.[32,35,42,43] Song et al.[28] reported the formation of core−shell morphologies for droplets of poly ethylene glycol (PEG)/AS/water droplets levitated in an electrodynamic balance (EDB) when elastic light scattering measurements were compared to Mie calculations for homogeneous and core−shell configurations.

We present studies of liquid−liquid phase separation in single aerosol droplets trapped using optical tweezers. In particular, we focus on two model systems for which data are available from particles deposited on surfaces, specifically PEG-400/AS and a mixture of C6-diacids/AS, a mixture of equal amounts (by mass) of 2-methylglutaric acid, 3-methylglutaric acid, and 2,2-dimethyl succinic acid. For the former system, bulk phase studies have also been performed that allow the calculation of spreading coefficients.[28] The main aim of this work is to determine if the phase separation behavior and compositional dependence of the separation RH of levitated droplets are consistent with the measurements reported from particles deposited on substrates. Furthermore, the sensitivity of the cavity-enhanced Raman spectroscopy technique to the refractive index and morphology of optically tweezed droplets will be used to gain insight into the morphology of liquid−liquid phase-separated aerosol particles.

II. EXPERIMENTAL DESCRIPTION AND ANALYSIS PROCEDURE

II.A. Bulk Measurements of Refractive Index and Phase Separation. To interpret the single-particle measurements presented later, it is important to first fully characterize the compositional dependence of the refractive indices of the mixed component solutions studied. Measurements of the refractive indices (RIs) of the mixed organic/inorganic (either PEG/AS or diacids/AS) aqueous solutions were made as a function of mass fraction of solute for the same OIR (mass ratios) used in the aerosol optical tweezers measurements described later. Measurements were first carried out at sufficiently high dilution and large mass fraction of water that phase separation had not occurred and the solutions could be considered homogeneous. Where possible, measurements of the RIs of both organic and aqueous phases were recorded for the more concentrated solutions that exhibited liquid−liquid phase separation. For these measurements, solutions were made up in a separating funnel and the two phases separated for refractive index measurement. All measurements on bulk solutions were carried out with a digital refractometer (Misco #PA203, wavelength of 589 nm). The water activity of each solution composition was calculated using the aerosol inorganic−organic mixtures functional groups activity coefficients (AIOMFAC) model,[44] based on knowledge of the exact masses of each solute and water forming the mixture. For the phase-separated solutions, the water activity is assumed to be the same as that for a homogeneous solution of the same composition calculated with AIOMFAC restricting the calculation to prevent phase separation. From the measured dependence of the refractive index on water activity, polynomial expressions were then used to describe the relationship between RI and water activity for each phase. These relationships between RI and water activity were then used to calculate the water activity of the single particles in the tweezers system at phase separation, with direct measurements of RI possible by this technique. Slightly different procedures were followed for the PEG:AS systems and the C6 acids:AS systems, as outlined below.

II.A.1. PEG:AS. For the PEG:AS system, a version of AIOMFAC optimized for the parametrization of polyethylene glycols[45] was used to calculate the water activity of each solution for which the RI was measured. The RI as a function of calculated water activity for each composition studied is shown in Figure 1, and the coefficients of the polynomial relationships

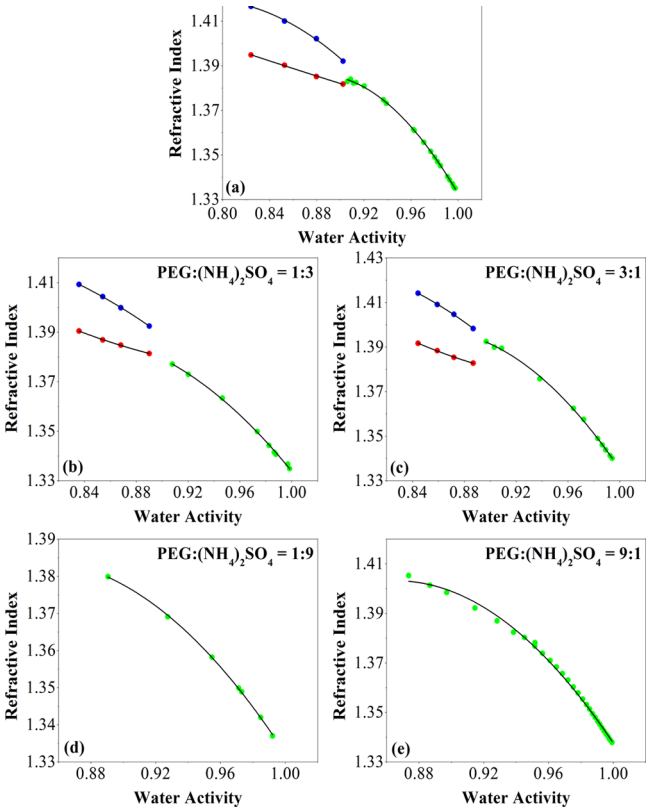

Figure 1. Bulk refractometer data showing refractive index at a wavelength of 589 nm as a function of water activity for the PEG:AS system (green points, single phase; blue points, organic phase; red points, inorganic phase; black lines, fits). Water activities calculated using AIOMFAC as detailed in the text.

are given in Table 1. The RI as a function of water activity is reported for solutions with dry mass solute ratios of 9:1, 3:1, 1:1, 1:3, and 1:9 (corresponding to OIR of 9, 3, 1, 0.33, and 0.11, respectively). Liquid−liquid phase separation is not

Table 1. Polynomial Coefficients for Relationship between Refractive Index (n) and Water Activity (a_w) for PEG/AS Solutions of Specified OIR[a]

composition (PEG:AS)	a	b	c
1:1	−21.078	55.520	−35.557
1:3	−17.954	46.581	−29.190
3:1	−16.970	44.553	−28.236
1:9	−27.533	72.469	−46.682
9:1	−20.403	54.184	−34.975

[a]In the form $a_w = an^2 + bn + c$ derived from experimental data in the temperature range of 20−23 °C for single-phase mixtures prior to phase separation.

DOI: 10.1021/acs.jpca.5b01658
J. Phys. Chem. A 2015, 119, 4177−4190

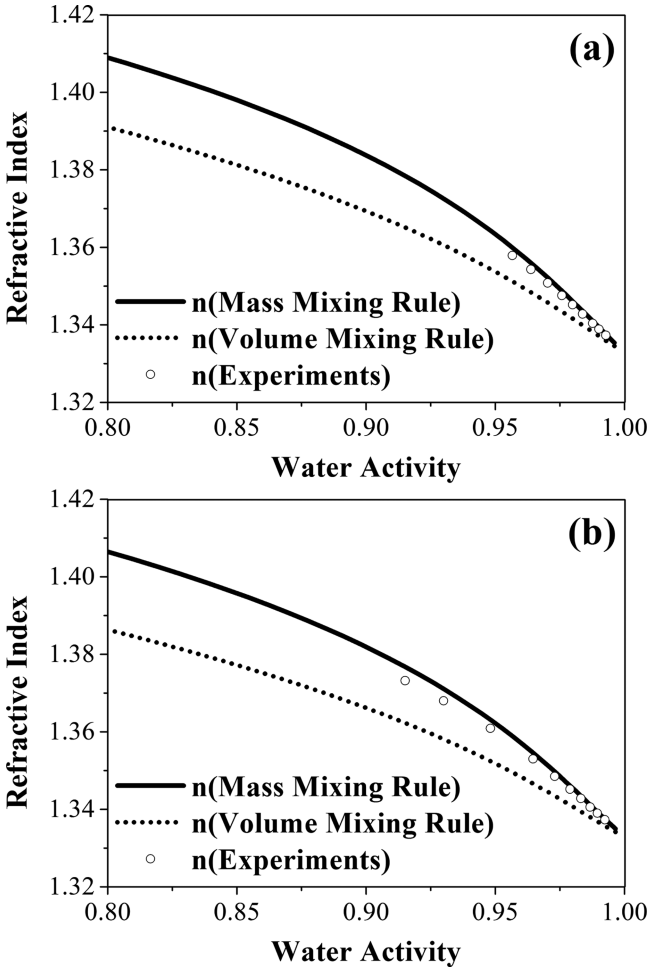

Figure 2. Bulk refractometer data (symbols) showing refractive index as a function of water activity for the C6-diacids:AS system. Water activities were calculated using AIOMFAC as detailed in the text. Measurements are compared with mass- and volume-weighted mixing rules as indicated. (a) Data for 1:2 dry mass ratio diacids:AS. (b) Data for 1:5 dry mass ratio diacids:AS.

observed for the bulk solutions in which the OIR is very high or very low. At intermediate OIR, phase separation is observed with the RI of the homogeneous solution just prior to phase separation tending to the RI of the dominant aqueous (inorganic-rich) or PEG (organic-rich) layer of the phase-separated solution. For solutions with a 1:1 PEG:AS dry mass ratio (OIR = 1), there is a clear discontinuity between the refractive index of the single phase and both the aqueous and organic layers.

II.A.2. C6-Diacids:AS. For this system, in which the organic component is an equal mass mixture of 2-methylglutaric acid, 3-methylglutaric acid, and 2,2-dimethylsuccinic acid, the standard web-based AIOMFAC model[44] was used in the same way as for the PEG:AS system. However, the bulk solubility limit was reached at water activities higher than that required for LLPS to occur because of the limited solubilities of these components. As a consequence, phase separation was not observed in the bulk measurements and the use of a polynomial relationship between the measured RI and calculated water activity would involve a large extrapolation to lower water activities to allow a direct estimation of the water activity at the SRH. To avoid this unconstrained extrapolation, the experimental RI were fitted to a variety of simple mixing rules derived from AIOMFAC data of solution properties as a function of water activity to allow a more robust and constrained calculation of the RI as a function of composition. The experimental data fitted best with the simple mass-weighted mixing rule (shown in Figure 2 with fit coefficients in Table 2), and the relationship between RI and water activity using this mixing rule was used to calculate the water activity from the measured RI at phase separation.

II.B. Single-Particle Measurements. The aerosol optical tweezers instrument coupled with Raman spectroscopy has been described in detail previously[46−48] and will only be summarized here. A gradient force optical trap is formed by focusing the light from a Nd:YVO_4 frequency-doubled laser (532 nm) through a 100× objective (numerical aperture of 1.25), with the light passing from the objective through a layer of immersion oil and then through a glass coverslip before entering the trapping cell. This creates an optical trap ∼40 μm above the microscope glass coverslip. Aerosol is introduced into the cell using a medical nebulizer (Omron MicroAIR Pocket Nebuliser), and any aerosol droplet that passes through the focal volume becomes trapped. The back-scattered Raman signal from the droplet is focused onto the entrance slit of a spectrograph equipped with a 1200 grooves per mm diffraction grating and a CCD array of 1024 × 256 pixels. The spectroscopic time resolution is 1 s. From the unique fingerprint of stimulated Raman scattering occurring at wavelengths commensurate with whispering gallery modes (WGMs), the refractive index and radius of the droplet can be derived with a high degree of accuracy by comparing the observed WGM positions to the predicted positions from Mie scattering calculations.[49]

In most experiments presented here, no active RH control was imposed and the trapped particles were allowed to dry as the RH declined to that of the ambient air. For some experiments, a slow (30 sccm) flow of dry nitrogen was passed through the cell to dry the trapped particle. Typical rates of RH change were 4% in 1000 s, and no dependence of the RH at

Table 2. Polynomial Coefficients for Relationship between Refractive Index (n) and Water Activity (a_w) for the C6-Diacids:AS System[a]

mixing rule	a	b	c	d	e	f
			1:2 C6-diacids:AS mass ratios			
mass	1.4952	−0.1798	0.7042	−2.0343	2.5322	−1.1833
volume	1.4913	−0.1981	0.5125	−1.292	1.5088	−0.6896
			1:5 C6-diacids:AS mass ratios			
mass	1.658	−1.7339	6.2207	−11.326	9.999	−3.4848
volume	1.5541	−0.8447	2.7884	−5.0827	4.5158	−1.5985

[a]In the form $n = a + ba_w + ca_w^2 + da_w^3 + ea_w^4 + fa_w^5$, derived from experimental data in the temperature range of 20−23 °C.

DOI: 10.1021/acs.jpca.5b01658
J. Phys. Chem. A 2015, 119, 4177−4190

phase separation on the rate of RH change was observed. Instead of measuring the RH using a capacitance probe, the water activity was inferred from the refractive index retrieved from the Raman measurement using the relationships between n and a_w obtained from the bulk measurements described earlier. In previous work we have shown that this approach allows the RH to be determined with an accuracy of better than ±0.1%, considerably more accurate that can be measured by a capacitance probe.[50] The temperature of the measurements was in the 20−23 °C range.

II.C. Fitting of WGMs in Raman Spectra to Homogeneous and Core−Shell Morphologies. The WGMs in the Raman spectra of homogeneous spheres were fitted using a previously described algorithm.[49] For the Raman spectra of core−shell particles, WGMs were fitted using a similar algorithm that had the following modifications: (i) the resonance condition was that of two concentric spheres and (ii) additional parameters were incorporated into the search space during the fitting. Full details of this will be described in a future publication.

Concerning the first difference, resonance combinations of particle size parameters (total radius and wavelength) and core and shell dimensions with independent RIs were identified by calculating the scattering coefficients for two concentric spheres over a wide range of trial solutions.[51] Resonances occur when a pole exists in the scattering coefficients and, as adopted previously,[49] the Newton−Raphson method was used to find the complex roots of the denominators of these coefficients. The main difficulty when employing a root-finding algorithm like the Newton−Raphson method is that suitable initial guesses are required. Here, guesses for the modes of interest were found by taking the resonances from a homogeneous sphere (calculated using the method in Preston and Reid[49]) and using these as initial guesses for the resonances for fitting the WGMs to a core−shell particle with a very thin shell. Once resonances had been identified for the particle with a thin shell, they could then be used as the initial guesses for the resonances of a core−shell particle with progressively thicker shells. This process was repeated until resonances were found for all shell thicknesses of interest. The assumption of this procedure is that small changes to shell thickness will result only in small changes to resonant size parameters.

The second difference between the fitting procedure used here and that used previously is that the search grid for the core−shell particle contains at least four parameters (if nothing is known beforehand about the core−shell particle): the radius of the shell, the radius of the core, the refractive index of the shell, and the refractive index of the core. Additionally, the inclusion of a linear dispersion term in both the refractive index of the core and shell may be needed if fits with higher accuracy are desired.[49] Therefore, in the absence of any prior information about the core−shell particle, it is necessary to generate and search a six-dimensional grid to find an accurate best fit. To reduce the computational demand, the linear dispersion term for both the core and the shell RIs was simply set to 15 nm^{-1}, a typical value from all of our previous work.[49] Additionally, for the fitted data presented in this publication, the RIs of the core and the shell at a fixed wavelength were chosen to be 1.385 and 1.400, the values at the water activities close to phase separation using the bulk data shown in Figure 1 for the PEG/AS system studied with an OIR of 0.33. By fixing the RIs with these values, it was then necessary to search only a two-dimensional grid which consisted of the radii of the two concentric spheres, allowing an approximate retrieval of the core radius and the shell thickness from the Raman spectra.

III. PHASE BEHAVIOR AND MORPHOLOGY FOR PEG/AS PARTICLES

III.A. Signatures of LLPS in Trapped Particles. It is first important to identify the possible signatures of liquid−liquid phase separation that arise when studying phase separation in optically tweezed aerosol droplets. The onset of liquid−liquid phase separation can be observed from the Raman spectra from the appearance of any one of three signatures, examples of which are shown in Figures 3−5. Briefly, the persistence of strong WGMs in the Raman fingerprint at phase separation accompanied by dramatic changes in their relative wavelengths provides a signature of phase separation to a morphology that retains spherical symmetry, but with a significant change in the radial profile in refractive index arising from the formation of a core−shell structure. Complete loss of the WGMs is consistent with a loss of spherical symmetry, a quenching of the high-quality WGMs of the previously spherical cavity, and the formation of a partially engulfed structure. Finally, a dramatic increase in the error associated with fitting the WGM structure, although more ambiguous, indicates the departure of the droplet from a homogeneous sphere and the possible formation of multiple inclusions or small distortions from sphericity.

III.A.1. Change in Mode Offset (CMO). Figure 3a shows examples of the Stokes-shifted Raman band from excitation of the O−H stretching vibration of water recorded from a mixed PEG/AS droplet undergoing phase separation. For a homogeneous droplet changing in size, the transverse electric modes (TE, a mode polarized with no radial dependence in the electric field) and transverse magnetic modes (TM, a mode polarized with no radial dependence in the magnetic field) shift in wavelength by very similar amounts with an approximately constant mode offset. The mode offset reflects the asymmetry in relative WGM wavelengths in the spectrum and is calculated from the wavelength of one TM mode, usually chosen to be a mode close to central within the Raman band, and the two neighboring TE modes of the same order and consecutive mode number. The mode order is defined by the number of maxima in the intensity of light in the radial coordinate and the mode number as the number of wavelengths of light forming a standing wave around the circumference of the droplet. The mode offset is identified by the quantity $|a - b|$ in Figure 3a. On undergoing LLPS to form a particle of core−shell morphology, the TE and TM modes shift by differing amounts,[43] showing a particularly dramatic change at the point at which the phase separation occurs; a core and a shell of significantly different refractive index are formed, leading to the sharp increase in mode offset apparent in Figure 3b.

Figure 3c shows how the fitting of the droplet radius and the refractive index deteriorate as the shell develops, resulting from a breakdown in the assumption that the particle is homogeneous when fitting the WGM fingerprint. The apparent sharp changes in the radius and refractive index retrieved from the Raman spectrum are not real and indicate phase separation has occurred. Additionally, the persistence of strong WGMs indicates that the morphology of the droplet remains spherical following LLPS and is core−shell. In the measurements reported below, the fitted refractive index immediately prior to LLPS has been used to infer the RH at phase separation; once phase separation starts (taking only a few seconds), the size and RI retrieved from the fit are in error and cannot be

DOI: 10.1021/acs.jpca.5b01658
J. Phys. Chem. A 2015, 119, 4177−4190

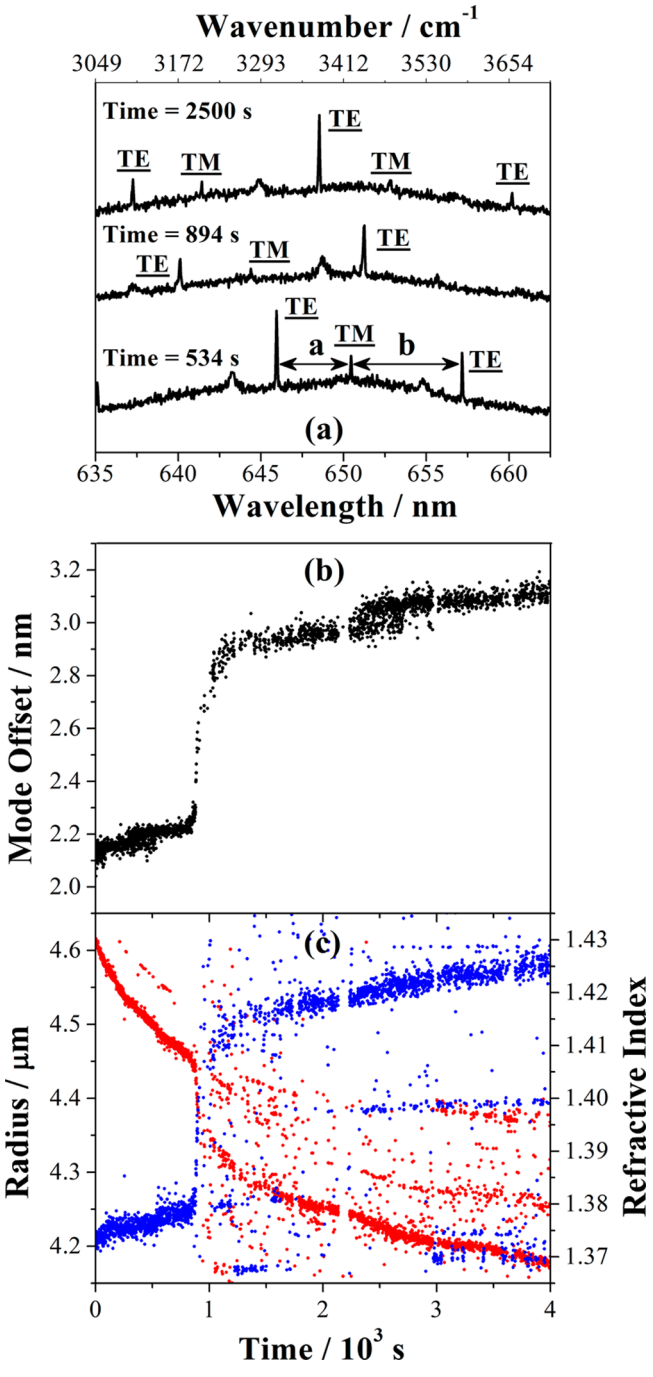

Figure 3. Example of identifying the mode offset (CMO) signature upon phase separation (PEG/AS system, organic-to-inorganic mass ratio OIR = 0.33). (a) Raman spectra before phase separation (534 s), just after phase separation (894 s), and when the mode offset has stabilized at higher value (2500 s). (b) Mode offset as a function of time. (c) Radius (red) and refractive index (blue) retrieved as a function of time.

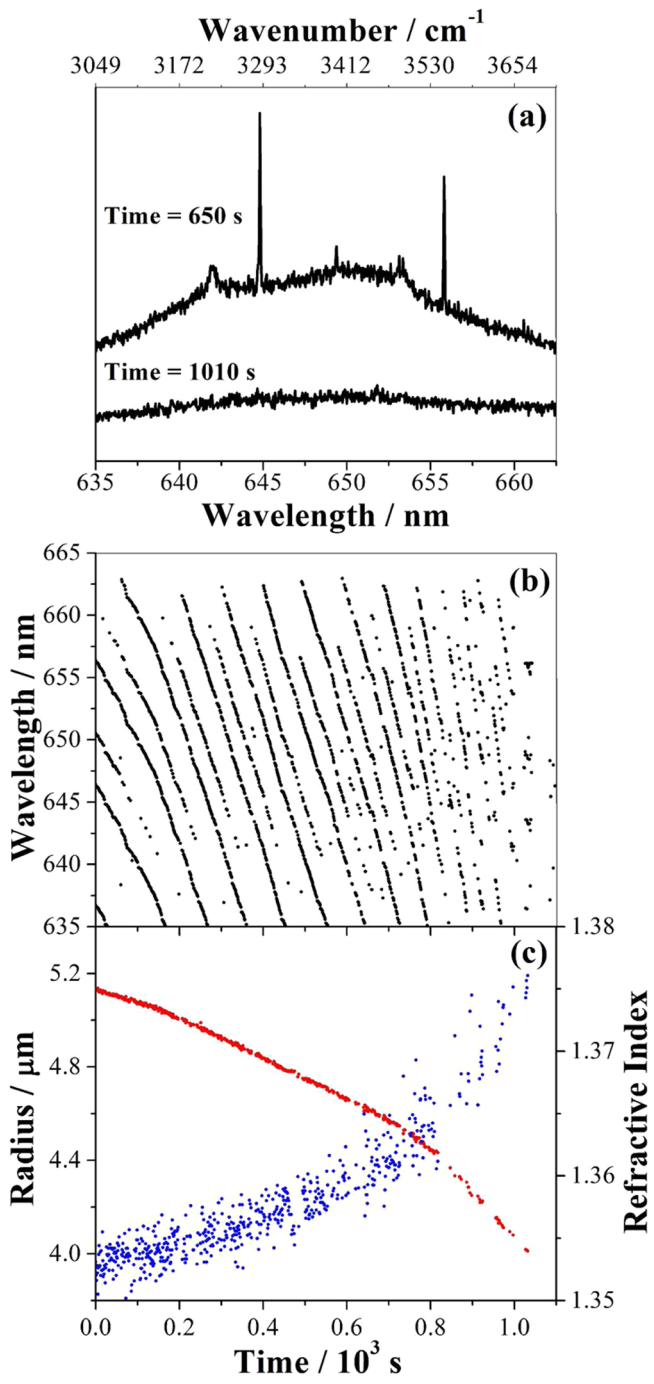

Figure 4. Example of identifying the mode quenching (QM) signature upon phase separation with the modes sporadic after phase separation (PEG/AS system, OIR = 3.00). (a) Spectra from the period before phase separation with whispering gallery modes (WGMs) present and just after separation showing mode quenching. Note that the spontaneous O−H Raman signal is still present although greatly diminished after phase separation. (b) Wavelengths of identified WGMs as a function of time. (c) Radius (red) and refractive index (blue) retrieved as a function of time.

used to infer the water activity at phase separation. For some of the experiments consistent with the formation of a core−shell morphology, the WGMs were compared with Mie simulations for droplets of core−shell morphology, allowing estimations of the core size and shell.

III.A.2. Quenching of WGMs (QM). In previous publications we have shown that LLPS can lead to the quenching of WGMs in the Raman spectrum, a consequence of the distortion in shape from a perfectly spherical resonator and the reduction of the high cavity quality factors usually associated with the WGMs for a droplet.[42,43] We observe similar behavior in a number of experiments in this study: as the particle diminishes in size, the WGMs became sporadic or even disappear completely, even though the particle remains trapped. An

DOI: 10.1021/acs.jpca.5b01658
J. Phys. Chem. A 2015, 119, 4177−4190

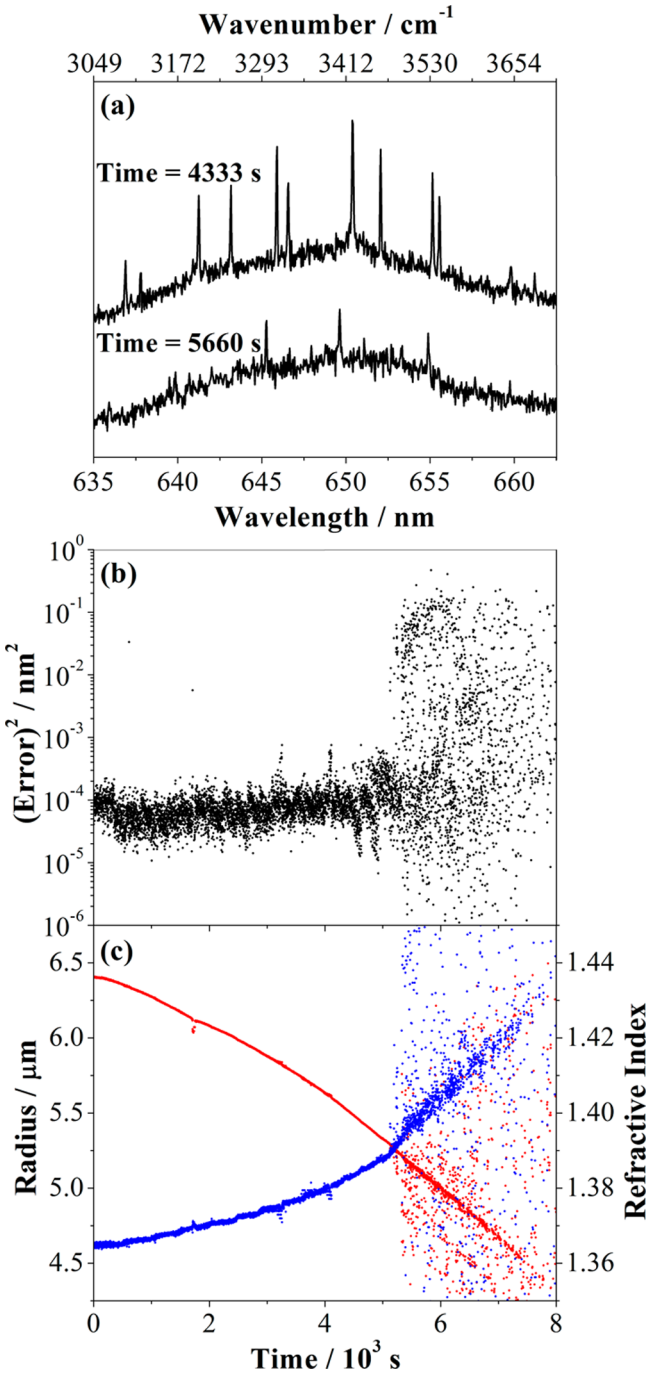

Figure 5. Example of identifying the increase in fitting error (IFE) signature upon phase separation with the WGM fingerprint no longer consistent with predictions for a homogeneous sphere (PEG/AS system, OIR = 3.00). (a) Spectra recorded before and after the increase in fitting error, both showing WGM fingerprints although with the modes diminished following phase separation. (b) The fitting error shows a considerable increase after phase separation (note the log scale). (c) Retrieved values of the droplet radius and refractive index assuming the droplet is homogeneous throughout.

example of this behavior is shown in Figure 4 for a PEG/AS particle: panel a shows two spectra, one taken before and another after phase separation. The wavelengths of the WGMs observed as a function of time are shown in panel b, and the results of the fitting of the WGM fingerprint to a homogeneous droplet are shown in panel c. As before, we conclude that the quenching of WGMs could be indicative of a distortion from sphericity due to phase separation and a morphology that is partially engulfed in which a lens of one phase at the surface of the particle disrupts the formation of WGMs. Such spectra could also be consistent with the formation of inclusions of ammonium sulfate within the droplet that move close to the surface, disrupting the modes.[52] This latter scenario can also explain why the intensity of the background spontaneous Raman OH band is considerably lower after the phase separation. In experiments that showed this behavior, phase separation was deemed to occur at the last frame where the spectra could be reliably and successfully fit to a homogeneous particle. The fitted refractive index was used to infer the RH at phase separation. It should be noted that following the apparent phase separation, WGMs can periodically reappear in the Raman spectrum but with intensity much lower than that for a homogeneous droplet (not shown in the figure), as apparent in Figure 4b.

III.A.3. Increase in Fitting Error (IFE). In a final class of experiment, WGMs continue to be observed with no significant increase in mode offset identified. However, the fitting error (the discrepancy between the measured wavelengths of the peaks and those calculated from Mie theory) is observed to increase by orders of magnitude. An example of this is shown in Figure 5: panel a shows spectra of the PEG/AS system (OIR = 3.0) recorded before and after the phase separation, panel b the fitting error as a function of time, and panel c the retrieved radius and refractive index of the droplet. Such observations can only be consistent with a breakdown in the assumption that the droplet is homogeneous, leading to inconsistency between the wavelengths of WGMs observed in the measurement and the predictions for a homogeneous droplet of any refractive index. Thus, an observation of increase in fitting error was assumed to indicate that the droplet was no longer homogeneous; indeed, it is most likely that the morphology is consistent with the presence of small inclusions of the aqueous phase moving around within the organic phase (similar to the QM case), but inclusions of a size that are unable to fully quench the high quality factor WGMs. The lowering of the quality of the WGMs leads to marginal increases in their line widths, a degradation in the determination of the resonant line centers, and an increase in the associated errors in the fitting. For accurate fits to a homogeneous droplet, the fitting error corresponds to an average error of ~0.01 nm/peak across all WGMs in the spectrum, reflecting the enhanced accuracy achieved from fitting the dispersed lineshapes (~0.04 nm/pixel) to a Gaussian when determining the line centers. Frame-to-frame fluctuations in the error become much larger after phase separation occurs, with some frames fitting by chance remarkably well and some showing large errors and a broadening in the retrieved droplet sizes and RIs from the fitting. Again, phase separation is deemed to occur at the last frame at which the pattern of WGMs is well represented by Mie simulations assuming homogeneity in composition. The average refractive index of the 10 frames preceding this is then used to determine the phase separation water activity. This assignment is not as robust as the previous two signatures of phase separation. Such behavior is consistent with previous observations of the elastic scattering measured from phase-separated droplets, in which distinct departures in elastic scattering from that expected for a homogeneous sphere were observed, but without a clear assignment in morphology possible.[28]

DOI: 10.1021/acs.jpca.5b01658
J. Phys. Chem. A 2015, 119, 4177−4190

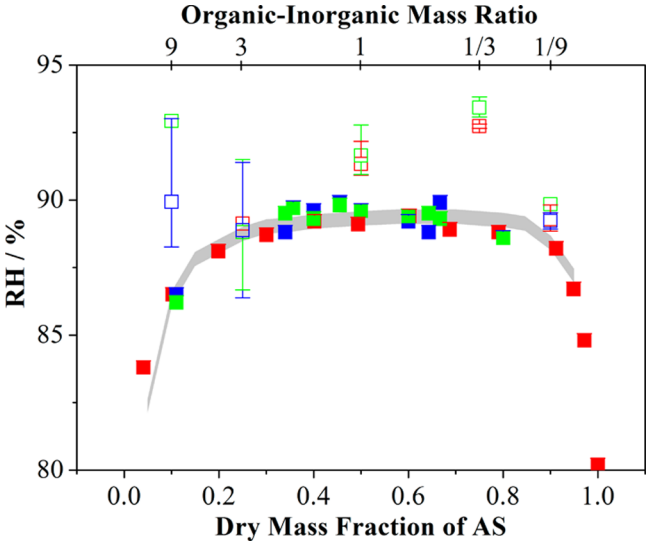

Figure 6. Phase-separation relative humidities observed from the PEG:AS single-particle measurements. The shaded region is the two-liquid phase−one-liquid phase boundary from the phase diagram presented by Ciobanu et al.[41] with the envelope indicating the range of uncertainty. Filled blue, green, and red squares indicate liquid−liquid phase separation RHs (SRHs) measured from microscope drying experiments,[18] microscope wetting experiments[18], and bulk phase experiments,[21] respectively. The red, green, and blue open squares show the averaged data from all phase separation RHs identified by CMO, QM, and IFE signatures, respectively. Error bars for this work show the range of SRHs obtained at each composition.

Table 3. Phase Separation RHs for All PEG-400:AS Droplets Studied and Signature of Phase Separation[a]

composition (PEG:AS)	phase separation RH (mean)	Phase separation RH (range)	signature
1:1	91.5	90.9−92.8	5 CMO; 6 QM; 0 IFE
1:3	93.2	92.6−93.8	2 CMO; 8 QM; 0 IFE
3:1	88.9	86.4−91.5	1 CMO; 6 QM; 2 IFE
1:9	89.2	88.6−89.8	9 CMO; 1 QM; 2 IFE
9:1	90.5	88.3−93.0	0 CMO; 1 QM; 4 IFE

[a]CMO, change in mode offset; QM, quenching of modes; IFE, increase in fitting error.

III.B. Compositional Dependence of the SRH. Using the signatures of phase separation described in the previous section, we report the observed phase separation humidities for PEG/AS mixtures inferred from the aerosol optical tweezers measurements in Figure 6. The bounded area indicates the range and uncertainty of phase separation RHs reported by Ciobanu et al.[41] for this system. In Table 3 we report the phase separation RHs and identify the signature of phase separation for each droplet studied. It is apparent that the single-particle data show phase separations at relative humidities between ∼86 and ∼94%, broadly consistent with, but marginally higher than, previous studies. It is, perhaps, surprising that the SRH from levitated droplets is marginally higher in some cases than the SRH of ∼85% to ∼91% reported for single particles deposited on coverslips. Bulk and single-particle measurements were performed in the range from 293 to 298 K. Although SRH depends on temperature, the dependency is minor in this limited temperature range and within the uncertainties of RH measurements. Also, in principle, the retrieval of the SRH is extremely accurate in the optical tweezers measurements given the accuracy with which the refractive index of the droplet just prior to phase separation can be determined. However, the estimated SRH does depend on the relationship of refractive index/mass fraction of solute to the water activity, and this is dependent on the accuracy of the thermodynamic relationship provided by bulk phase data with measurement accuracies typically of ±0.3% RH.[21,41] Some of our bulk phase measurements of RI show liquid−liquid phase separation at RHs between our optical tweezers measurements and the previously published values, reflecting the pronounced dependencies on environmental parameters and composition that exist. The low variability in the refractive indices at phase separation (and, thus, the precision on the SRH determinations) must reflect the intrinsic variability in the separation relative humidities of different droplets and compositions rather than resulting from the more typical random error in measurement of the gas phase RH typical of most measurements. We will return to this point when we describe the reproducibility of the SRH recorded for the same droplet on repeated drying and humidifying cycles and, thus, repeated phase separation cycles. We first present a brief summary of the results for each composition.

III.B.1. 1:1 PEG-400:AS by Mass (OIR = 1). For single particles of this composition, phase separation occurred at relative humidities between 90.9 and 92.8%, slightly higher than the data presented by Ciobanu et al.[41] for particles deposited on coverslips and bulk data. In Figure 6, single-particle data are presented for 11 particles, 5 of which showed a clear increase in mode offset (CMO) and 6 of which showed phase separation by a breakdown in the homogeneous particle fitting (IFE) as described in section III.A.

III.B.2. 1:3 PEG:AS by Mass (OIR = 0.33). Liquid−liquid phase separation was observed to occur between 92.6 and 93.8% relative humidity, higher than the range indicated in the work of Ciobanu et al.[41] Data are presented in Figure 6 for 10 particles, 2 of which showed a marked increase in mode offset (CMO behavior); 8 showed a breakdown in the fit and sporadic WGMs (QM behavior).

III.B.3. 3:1 PEG:AS by Mass (OIR = 3). Liquid−liquid phase separation was observed to occur between relative humidities of 86.4 and 91.5%, in excellent agreement with the Ciobanu[41] data, although our measurements for this composition exhibit a range of variability in phase separation RH that is larger than that for other compositions. In Figure 6, data are presented for nine single particles only one of which showed a mode offset increase (CMO). Of the remainder, six showed QM behavior and the remaining two particles showed IFE behavior.

III.B.4. 1:9 PEG:AS by Mass (OIR = 0.11). Phase separation was observed to occur between 88.6 and 89.8% RH, again in excellent agreement with previous work on particles deposited on substrates and with bulk measurements that showed LLPS at 88.4% RH.[41] Data are presented in Figure 6 for 12 single particles, 9 of which show CMO behavior; 1 shows QM behavior, and 2 show IFE behavior.

III.B.5. 9:1: PEG:AS (OIR = 9). For these organic-rich droplets, LLPS was observed over a RH range much larger than that of the other compositions, extending from 88.3 to 93.0% RH. However, of the five particles for which data are presented in Figure 6, none of these particles exhibited CMO behavior and

DOI: 10.1021/acs.jpca.5b01658
J. Phys. Chem. A 2015, 119, 4177−4190

only one exhibited QM behavior. The remaining droplets were determined to have phase-separated through an observed increase in the fitting error (IFE, the least robust indicator of phase separation), and as such these data should be treated with caution. We shall return to the reasons for the apparent dominance of this form of phase separation indicator below.

Given that the data for droplets of the 9:1 PEG:AS solution are the least reliable, agreement of the SRH between this study and the previous bulk phase measurements and studies of droplets on coverslips is within 4% with an enhanced asymmetry with inorganic-rich solutions showing a higher SRH, particularly the 1:3 PEG:AS solution. There is no systematic dependence of the SRH on the signature of LLPS. Again, it should be stressed that the narrow range (high precision) of SRHs reported indicates a true level of variability droplet to droplet.

III.C. Comparison of Reproducibility in SRH for Different Particles and the Same Particle. As can be seen from Table 3, the variability in separation relative humidity between different particles of the same composition is generally within 2−3% RH for sulfate-rich particles and within ∼5% for PEG-rich particles. The high degree of precision with which the refractive index at phase separation is inferred from the refractive index indicates that the range of values observed over numerous droplets reflects the real variability in composition at phase separation from droplet to droplet rather than uncertainty in an experimental variable such as RH. To support this conclusion, a single particle was repeatedly passed through the phase transition on a number of RH cycles, repeatedly switching between a homogeneous single-phase droplet and a droplet with LLPS. If it is correct that the tweezers measurements are sufficiently precise to distinguish between the small (but real) differences in phase separation RH between different particles, it would be expected that the same particle should show a degree of variation in SRH smaller than is observed between the particles shown in Figure 6 and Table 3.

Figure 7 reports the results from the repeated cycling of the same 1:3 PEG:AS (OIR = 0.33) particle through the phase separation RH, both through drying and humidifying cycles. It is immediately apparent from the mode offset data (CMO) that phase separation and remerging to one phase occur on repeated cycles, and this is supported by the error in the spectral fitting (IFE), which shows excellent correlation with the CMO signature. A breakdown in the assumption of homogeneity in refractive index is indicated by both the CMO and IFE signatures. It should also be noted that the noise in the time series of radius and refractive index also increases upon phase separation for the same reason and that the apparent change in radius and refractive index when separation occurs is simply an artifact of the breakdown of this assumption.

The exact times at which phase separation and the return to one phase occur are not possible to define; instead, phase transitions occur over narrow periods in time. In identifying these periods, we note the following. First, before the first clear discontinuity in slope and increase in error, mode offset and radius at ∼2500 s (Figure 7), the error increases and the mode offset cannot be calculated from ∼1700 s. This is a consequence of a diminution of mode intensities to a point where first-order TM modes are no longer sufficiently intense and sharp to determine a mode offset, but the persistence of first and second-order TE modes ensures that fitting can be achieved, albeit with larger errors. This is possibly a consequence of some initial phase separation with formation of very small inclusions

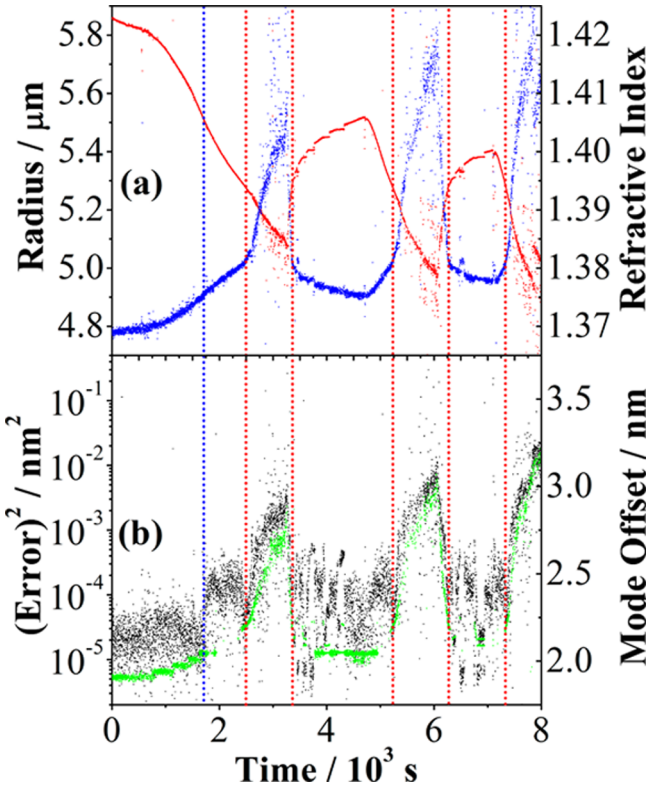

Figure 7. Repeated cycles of the same 1:9 dry mass PEG-400/AS droplet through the phase separation RH showing the reproducibility in the composition of the droplet (as inferred from refractive index) at phase separation. The vertical red lines indicate the times at which a phase transition occurs with the blue vertical line indicating a transition in the spectrum that is not commensurate with an unambiguous phase transition but does suggest some qualitative change in homogeneity and mixing state. (a) Time dependence of radius (red) and refractive index (blue). When the droplet has separated into two phases, the reported radii and refractive indices retrieved from homogeneous fits to the spectra should not be taken as correct. (b) Time dependence of mode offset (green) and error (black). The size, RI, and water activity at each phase separation is reported in Table 4.

that partially quench modes; however, it is not possible to convincingly identify this point as the time of phase separation. Instead, all four signatures (radius, RI, error, and mode offset) show consistent and sudden changes at ∼2500 s, and we report this point as being the time at which liquid−liquid phase separation occurs. On humidifying, the error and mode offset never return to the consistently low values seen at the very beginning of the experiment, suggesting that a completely homogeneous phase is never fully re-established but small inclusions may persist. Similar abrupt changes occur on subsequent drying cycles at ∼5230 and ∼7300 s, and we report the droplet sizes, RIs, and RHs at these times in Table 4. Given the very slow rate at which the RH is changing, uncertainties are small, but we report ranges for each of these quantities based on the time period between which the error first increases above 1×10^{-2} nm to when it increases above 2×10^{-2} nm, typically a period of 50 s. Although a rather arbitrary choice, our purpose here is to look at the reproducibility in the behavior of the droplet from one cycle to the next. This error also corresponds approximately to an increase in the average error in reproducing the resonant wavelengths in the Raman spectrum from less than one pixel on

DOI: 10.1021/acs.jpca.5b01658
J. Phys. Chem. A 2015, 119, 4177−4190

Table 4. Reproducibility in the Phase Separation Cycles for a Single Particle, 3:1 PEG:AS, Showing the Ranges in Inferred Size, Refractive Index, and Water Activity at Phase Separation

	radius (μm)		n		a_w	
	initial	final	initial	final	initial	final
initial phase separation	5.254	5.228	1.3830	1.3862	0.9225	0.9147
first return to one phase	5.215	5.266	1.3887	1.3825	0.9083	0.9237
second phase separation	5.248	5.231	1.3835	1.3851	0.9213	0.9174
second return to one phase	5.228	5.270	1.3876	1.3825	0.9111	0.9237
third phase separation	5.240	5.202	1.3836	1.3885	0.9210	0.9088

the CCD on average to more than one. At times after these, fitting to a homogeneous Mie calculation leads to clear errors in representing the light scattering from the droplet. The same change in error, decreasing from 2×10^{-2} to 1×10^{-2} nm, is used to define the time period over which the two phases merge to form a droplet formed predominantly from one phase.

Some trends in the radii, RIs, and water activities are clear in Table 4. The ranges of radii, RIs, and water activities are consistent with each other for either phase separation or the return to one phase. Differences in the initial and final water activities reported are within a range of ±0.1% and ±0.5% RH, respectively, for phase separation. While the first point in the range is fairly well-defined, the final point is less defined. For the return to one phase, the two measurements of the final water activity (now the most well-defined) are in perfect agreement while the initial water activities differ by only 0.3% RH. Most clearly, the water activities at which the error in the fitting crosses the 0.01 nm threshold agree to within a standard deviation of ±0.13% RH across all five transitions. From these measurements, the variability of composition and SRH determined for repeated measurements on the same particle is much smaller than the variability between particles. Although the data reported here are for a single particle, the one for which we have the most comprehensive set of data, similar behavior has been observed for numerous droplets. This supports our conclusion that each particle shows a distinct (and slightly different) SRH but that there is considerable variability between particles. The reasons for variability between particles at the same composition are not clear as they are prepared by nebulizing the same bulk solution. In addition, no obvious correlation could be found between SRH and particle radius, rate of drying, or length of experiment.

III.D. Morphology of Liquid–Liquid Phase-Separated Particles. Ciobanu et al.[41] identified the initial process by which phase separation occurs from the imaging of particles at the onset of phase separation in their microscope images of particles deposited on surfaces. Their data indicate that phase separation occurred by the formation of aqueous inclusions for particles with a high OIR of 8:1 to 2:1. In particles with low OIR (1:2 to 1:8), phase separation occurred by growth of a second organic-rich phase from the particle's rim. At intermediate OIR, phase separation developed by the formation of schlieren which eventually coalesced into aqueous inclusions. These observations seem to imply that particles rich in sulfate should separate into core–shell particles (the formation of an organic-rich layer from the surface). Conversely, as the proportion of the organic component in the droplet increases, the tendency to separate through the formation of inclusions within the droplet was observed.

From Table 3 it is clear that the very sulfate-rich particles (OIR = 0.11) show predominantly CMO behavior, consistent with the formation of a thin shell at the surface of the particle. In particles with a very low mass fraction of sulfate (OIR of 3 and higher), the results show the particles are more likely to show QM or IFE behavior on separation, consistent with the formation of inclusions within the droplet moving around and quenching the appearance of WGMs or with the formation of a partially engulfed structure. At the intermediate OIRs studied in this work, the data seem to be fairly evenly split between CMO and QM type behavior, possibly indicating some degree of competition between these two mechanisms with a stochastic element determining which is the initiating factor. The data on levitated single particles in this study, therefore, seem to broadly validate the observations of Ciobanu et al.[41] for the very aqueous-rich and organic-rich particles, but with some ambiguities arising in the particles of intermediate OIR. In this study, *all* of the particles that lost sufficient water to reach the SRH showed LLPS, as did those observed by Song et al.[28] for particles of the same compositions.

For particles which show CMO behavior, we have investigated the plausibility of fitting the WGM fingerprints to a core–shell structure rather than a homogeneous droplet, potentially allowing a determination of the refractive index and radius of the core as well as the refractive index of the shell and the shell thickness. Fitting of all four parameters independently is computationally expensive. Instead, the refractive indices of the core and shell are fixed at values representative of the expected values at the water activity corresponding to the SRH, as discussed in section II.C. Then, the radius of the core and thickness of the shell are varied to obtain a best fit for the observed WGM fingerprint. Results for core–shell fitting are shown in Figure 8 for a particle (PEG:AS 1:3; OIR = 0.33) which started as a homogeneous particle, phase separated into a core–shell morphology at a time of 878 s, and then reformed a homogeneous particle again at a time of 38 783 s. As the figure shows, the shell develops and increases in thickness to 100 nm before decreasing again and disappearing as the particle returns to one phase. The film thickness is ∼2.5% of the particle radius at a maximum, corresponding to a volume ratio of the aqueous AS core to total droplet volume, $V(\mathrm{AS})/V(\mathrm{tot})$, of 0.93.

The ratio $V(\mathrm{AS})/V(\mathrm{tot})$ that would be expected from thermodynamic predictions can be calculated using AIOMFAC to calculate the compositions of PEG/water and AS/water phases at a range of RHs close to the SRH observed for particles of this composition. The results of these calculations, as well as the experimental data from the core–shell fitting, are shown in Figure 8b. It is apparent that the volume ratio derived from the Raman spectra is close to that calculated using AIOMFAC at 94% RH (the SRH observed in the tweezers system) shown by the middle line in Figure 8b. The upper line (AIOMFAC calculation for 96% RH) and lower line (AIOMFAC calculation for 92% RH) are shown to give an idea of the sensitivity of these calculations to RH. The slight underestimation in the calculation by ∼1.5% may be due to incomplete phase separation, i.e., that none of the organic component remains in the aqueous phase. The estimation, based on AIOMFAC calculations, assumes that complete phase separation occurs. This may not be a good assumption close to

DOI: 10.1021/acs.jpca.5b01658
J. Phys. Chem. A 2015, 119, 4177–4190

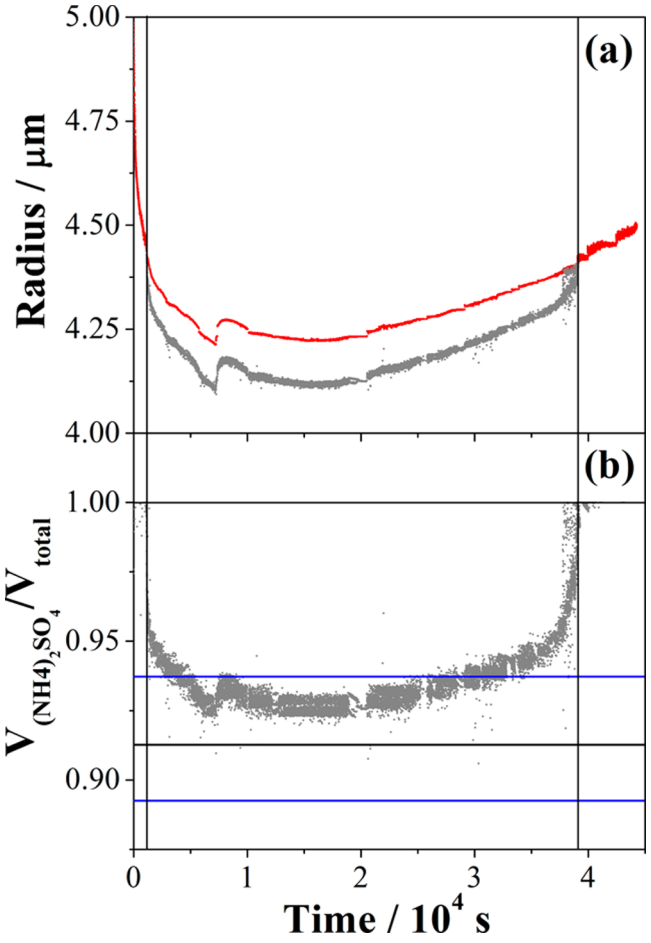

Figure 8. (a) Total radius of droplet (red) and radius of core (gray) for a particle with OIR = 0.33. Black vertical lines mark start and end of LLPS. Prior to 878 s and liquid−liquid phase separation, the WGM fingerprint is accurately represented by fits to a homogeneous spherical droplet; fitting to a core−shell structure need not be considered. After this time, the droplet phase separates into a core−shell structure with an aqueous inorganic core assumed to have a refractive index of 1.385 and an organic shell of refractive index 1.392. After 38 783 s, the WGM fingerprint once again is consistent with a homogeneous droplet without phase separation. (b) From the radius of the core and the total droplet size, the volume fraction of the inner aqueous phase can be calculated and compared with the overall volume of the droplet. This volume fraction is consistent with expectations of the volume ratio of the aqueous inorganic and organic phases calculated from AIOMFAC (black horizontal line) based on phase separation at a relative humidity of 94%, as inferred from the refractive index at phase separation determined from the homogeneous fitting prior to the signature of phase separation. The upper and lower blue lines indicate the volume ratios that would be expected from AIOMFAC if the phase separation occurred at SRHs of 96% or 92%, respectively.

the onset of phase separation and may account for the discrepancy: close to separation, a significant proportion of the PEG may still reside in the core aqueous phase. We should also note that we have assumed particular values for the RIs of the aqueous and organic phases to perform the core−shell fitting, potentially introducing some error into the radii of the core and shell.

IV. PHASE BEHAVIOR AND MORPHOLOGY FOR MIXED C6-DIACIDS/AS PARTICLES

In this system, the organic component is a mixture containing equal amounts (by mass) of 2-methylglutaric acid, 3-methylglutaric acid, and 2,2-dimethylsuccinic acid. These organic components formed one of the mixtures of complex composition chosen by Song et al.[15] to better reflect the complexity observed in atmospheric aerosol and to have O:C ratios similar to compounds observed in ambient aged secondary organic aerosol. Song et al.[15] observed SRHs significantly lower than those observed for the aqueous PEG-400/AS system and found that both core−shell and partially engulfed morphologies could form upon LLPS. This system therefore allows a second direct comparison between droplets deposited on coverslips and optically trapped droplets under drier conditions with a morphology dependent on RH.

The SRH estimated from measurements made with this system are reported in Figure 9. The signifier of phase separation (as defined in section III.B) is identified in each case. Also shown are the data points from Song et al.[15] and a shaded area indicating the range of compositions and separation humidities for aerosol richer in the inorganic component presented in the same paper. It is immediately apparent that the data presented for this work show phase separation at relative humidities higher than those reported by Song et al.[15] This may be due to inaccuracies in the mass mixing rule used to calculate the water activity from the refractive index at phase separation in this work. The variability of the relative humidity at phase separation (~5−6% RH) between particles is comparable to that in the PEG:AS system, again indicating a small but real difference in the behavior of individual particles of the same composition.

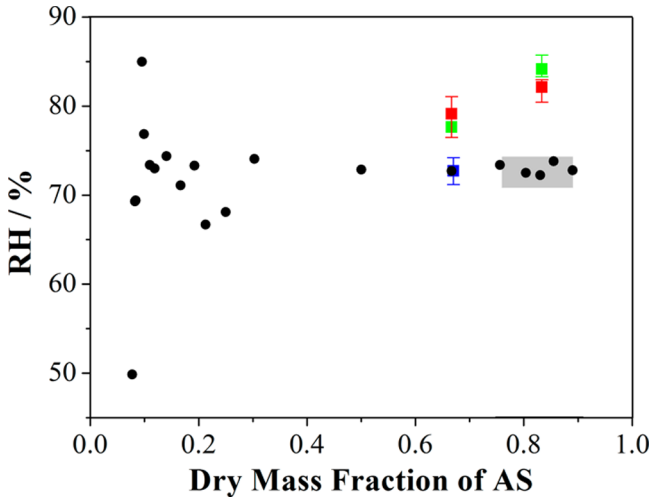

Figure 9. Liquid−liquid phase separation RHs measured for droplets consisting of the C6-diacids:AS solution of two mass ratios. The red and green symbols show the averaged data from all phase separation RHs identified by CMO and QM signatures, respectively, and error bars show the range of SRH obtained at each composition. The blue data point is the SRH from Song et al.[15] Data points from the same work (shown as filled black circles) give a SRH range of 72.3−72.8 for a dry mass fraction of AS (balance C6-diacids) range of 0.76−0.89, as indicated by the gray box which also indicates the quoted 1.5% error bar in RH.

Over the narrow composition range shown in Figure 9 our work indicates a number of particles that show CMO type

DOI: 10.1021/acs.jpca.5b01658
J. Phys. Chem. A 2015, 119, 4177−4190

behavior (nine particles; indicative of core−shell morphology) slightly higher than QM type behavior (five particles; indicative of partially engulfed morphology or inclusions within the particle), although both compositions show both types of behavior. For this system, Song et al.[15] observed the formation of aqueous ammonium sulfate inclusions, some of which merged over time, with the more major inclusions moving toward the droplet edge, behavior that would be consistent with the eventual observation of a QM signature.

IV. CONCLUSIONS

Data is presented showing how the relative humidity at which liquid−liquid phase separation occurs varies with composition for single levitated particles containing PEG-400/ammonium sulfate/water and a mixture of C6-diacids/ammonium sulfate/water. In the PEG/AS system, the observed SRH in the optical tweezers is in general agreement (albeit slightly higher for some compositions) with the data of Ciobanu et al.[41] which indicated liquid−liquid phase separation in droplets of the same compositions deposited on hydrophobic substrates, indicating the substrate does not have an appreciable effect on the relative humidity at which separation occurs for this system. For the diacid system, the phase separation relative humidities derived from this work are higher than those presented by Song et al.,[15] again inferred from measurements on substrates.

The morphology of the particles has also been investigated using characteristic changes in the Raman spectra of the droplets to infer phase changes of the particle. In the PEG system, at high AS content the droplets predominantly form core−shell particles; at high PEG content it appears the spectra are more consistent with a morphology consisting of small inclusions of an aqueous phase dispersed in the organic phase or partially engulfed structure. However, in all cases, a mixture of indicators is observed for phase separation and the indicators fluctuate over time, suggesting that the morphology may not be constant and that different morphologies may be adopted depending on exact volume ratios, RH, and composition. This is consistent with simulations from an early framework developed to predict the morphology in which the energy differences between different structures can be very small.[33] Our measurements suggest a distinction between two mechanisms of LLPS at the onset of phase separation with CMO type behavior at low OIR indicating the formation of a thin organic shell at the surface and QM type behavior indicating the formation of aqueous inclusions which may go on to form an aqueous core. These findings are in agreement with those of Ciobanu et al.[41] and Song et al.[15] For particles exhibiting core−shell morphology we have retrieved the shell thickness from the wavelengths of the WGMs in the Raman spectra, results that compare well with estimates of the expected film thickness using AIOMFAC to estimate the water associated with ammonium sulfate and PEG-400 and thus the volume ratio of the two phases. The experimental data marginally underestimate the film thickness, but this may be due to the incomplete partitioning of PEG from the aqueous AS core into the shell over the finite time scale of the measurement. For the C6 diacid system, our results imply that over the narrow composition range studied core−shell, satellite inclusions, and partially engulfed morphologies are possible. This is again in broad agreement with the work of Song et al.[15] which indicated that after phase separation partial coalescence led to the formation of a major inner inclusion together with satellite inclusions. At a lower RH, the major inner inclusion tended to move from the core to the edge of the particle, leading to a partially engulfed configuration.[15]

AUTHOR INFORMATION

Corresponding Author

*E-mail: j.p.reid@bristol.ac.uk.

Notes

The authors declare no competing financial interest.

ACKNOWLEDGMENTS

J.P.R. and D.J.S. acknowledge financial support from the EPSRC through the support of a Leadership Fellowship (EP/G007713/1) awarded to J.P.R. T.C.P. acknowledges the National Science and Engineering Research Council of Canada for funding as a postdoctoral research fellow. C.C. acknowledges support from the China Scholarship Council. Y.H.Z. acknowledges support from the NSFC (41175119, 21373026, and 21473009) and 111 project (B07012). Prof. A. Zuend (McGill University) is acknowledged for providing thermodynamic calculations for the PEG/AS system.

REFERENCES

(1) Ravishankara, A. R. Heterogenous and Multiphase Chemistry in the Troposphere. *Science* **1997**, *276*, 1058−1065.
(2) Kolb, C. E.; Worsnop, D. R. Chemistry and Composition of Atmospheric Aerosol Particles. *Annu. Rev. Phys. Chem.* **2012**, *63*, 471−491.
(3) IPCC. *Climate Change 2007: The physical science basis. Contribution of Working Group I to the Fourth Assessment Report on the Intergovernemental Panel on Climate Change*; Cambridge University Press: New York, 2007.
(4) Twomey, S. Aerosols, Clouds and Radiation. *Atmos. Environ., Part A* **1991**, *25*, 2345−2442.
(5) Carslaw, K. S.; Lee, L. A.; Reddington, C. L.; Pringle, K. J.; Rap, A.; Forster, P. M.; Mann, G. W.; Spracklen, D. V.; Woodhouse, M. T.; Regayre, L. A.; Pierce, J. R. Large Contribution of Natural Aerosols to Uncertainty in Indirect Forcing. *Nature* **2013**, *503*, 67−71.
(6) Lohman, U.; Feichter, J. Global Indirect Aerosol Effects: A Review. *Atmos. Chem. Phys.* **2005**, *5*, 715−737.
(7) Stevens, B.; Feingold, G. Untangling Aerosol Effects on Clouds and Precipitation in a Buffered System. *Nature* **2009**, *461*, 607−613.
(8) Hanel, G. Single-Scattering Albedo of Atmospheric Aerosol-Particles as a Function of Relative Humidity. *J. Atmos. Sci.* **1976**, *33*, 1120−1124.
(9) Martin, S. T. Phase Transitions of Aqueous Atmospheric Particles. *Chem. Rev. (Washington, DC, U.S.)* **2000**, *100*, 3403−3454.
(10) Wall, S. M.; John, W.; Ondo, J. L. Measurement of Aerosol Size Distributions for Nitrate and Major Ionic Species. *Atmos. Environ.* **1988**, *22*, 1649−1656.
(11) Krieger, U. K.; Marcolli, C.; Reid, J. P. Exploring the Complexity of Aerosol Particle Properties and Processes using Single Particle Techniques. *Chem. Soc. Rev.* **2012**, *41*, 6631−6662.
(12) Shiraiwa, M.; Seinfeld, J. H. Equilibration Timescale of Atmospheric Secondary Organic Aerosol Partitioning. *Geophys. Res. Lett.* **2012**, *39*, L24801.
(13) Marcolli, C.; Luo, B. P.; Peter, Th.; Wienhold, F. G. Internal Mixing of the Organic Aerosol by Gas Phase Diffusion of Semivolatile Organic Compounds. *Atmos. Chem. Phys.* **2004**, *4*, 2593−2599.
(14) Bertram, A. K.; Martin, S. T.; Hanna, S. J.; Smith, M. L.; Bodsworth, A.; Chen, Q.; Kuwata, M.; Liu, A.; You, Y.; Zorn, S. R. Predicting the Relative Humidities of Liquid-Liquid Phase Separation, Efflorescence, and Deliquescence of Mixed Particles of Ammonium Sulfate, Organic Material, and Water using the Organic-to-Sulfate Mass Ratio of the Particle and the Oxygen-to-Carbon Elemental Ratio of the Organic Component. *Atmos. Chem. Phys.* **2011**, *11*, 10995−11006.

DOI: 10.1021/acs.jpca.5b01658
J. Phys. Chem. A 2015, 119, 4177−4190

(15) Song, M.; Marcolli, C.; Krieger, U. K.; Zuend, A.; Peter, T. Liquid-Liquid Phase Separation and Morphology of Internally Mixed Dicarboxylic Acids/Ammonium Sulfate/Water Particles. *Atmos. Chem. Phys.* **2012**, *12*, 2691−2712.
(16) Marcolli, C.; Luo, B. P.; Peter, T. Mixing of the Organic Aerosol Fractions: Liquids as the Thermodynamically Stable Phases. *J. Phys. Chem. A* **2004**, *108*, 2216−2224.
(17) Parsons, M. T.; Riffell, J. L.; Bertram, A. K. Crystallization of Aqueous Inorganic-Malonic Acid Particles: Nucleation Rates, Dependence on Size, and Dependence on the Ammonium-to-Sulfate Ratio. *J. Phys. Chem. A* **2006**, *110*, 8108−8115.
(18) Ciobanu, V. G.; Marcolli, C.; Krieger, U. K.; Zuend, A.; Peter, T. Efflorescence of Ammonium Sulfate and Coated Ammonium Sulfate Particles: Evidence for Surface Nucleation. *J. Phys. Chem. A* **2010**, *114*, 9486−9495.
(19) Smith, M. L.; Kuwata, M.; Martin, S. T. Secondary Organic Material Produced by the Dark Ozonolysis of α-Pinene Minimally Affects the Deliquescence and Efflorescence of Ammonium Sulfate. *Aerosol Sci. Technol.* **2011**, *45*, 244−261.
(20) Smith, M. L.; Bertram, A. K.; Martin, S. T. Deliquescence, Efflorescence, and Phase Miscibility of Mixed Particles of Ammonium Sulfate and Isoprene-Derived Secondary Organic Material. *Atmos. Chem. Phys.* **2012**, *12*, 9613−9628.
(21) Marcolli, C.; Krieger, U. K. Phase Changes During Hygroscopic Cycles of Mixed Organic/Inorganic Model Systems of Tropospheric Aerosols. *J. Phys. Chem. A* **2006**, *110*, 1881−1893.
(22) Virtanen, A.; Joutsensaari, J.; Koop, T.; Kannosto, J.; Yili-Pirila, P.; Leskinen, J.; Makela, J. M.; Holopainen, J. K.; Pöschl, U.; Kulmala, M.; Worsnop, D. R.; Laaksonen, A. An Amorphous Solid State of Biogenic Secondary Organic Aerosol Particles. *Nature* **2011**, *467*, 824−827.
(23) Pfrang, C.; Shiraiwa, M.; Pöschl, U. Chemical Ageing and Transformation of Diffusivity in Semi-Solid Multi-Component Organic Aerosol Particles. *Atmos. Chem. Phys.* **2011**, *11*, 7343−7354.
(24) Koop, T.; Bookhold, J.; Shiraiwa, M.; Pöschl, U. Glass Transition and Phase State of Organic Compounds: Dependency on Molecular Properties and Implications for Secondary Organic Aerosols in the Atmosphere. *Phys. Chem. Chem. Phys.* **2011**, *13*, 19238−19255.
(25) Bones, D. L.; Reid, J. P.; Lienhard, D. M.; Krieger, U. K. Comparing the Mechanism of Water Condensation and Evaporation in Glassy Aerosol. *Proc. Natl. Acad. Sci. U.S.A.* **2012**, *109*, 11613−11618.
(26) Song, M.; Marcolli, C.; Krieger, U. K.; Zuend, A.; Peter, T. Liquid-Liquid Phase Separation in Aerosol Particles: Dependence on O:C, Organic Functionalities, and Compositional Complexity. *Geophys. Res. Lett.* **2012**, *39*, L19801.
(27) You, Y.; Smith, M. L.; Song, M.; Martin, S. T.; Bertram, A. K. Liquid−Liquid Phase Separation in Atmospherically Relevant Particles Consisting of Organic Species and Inorganic Salts. *Int. Rev. Phys. Chem.* **2014**, *33*, 43−77.
(28) Song, M.; Marcolli, C.; Krieger, U. K.; Lienhard, D. M.; Peter, T. Morphologies of Mixed Organic/Inorganic/Aqueous Aerosol Droplets. *Faraday Discuss.* **2013**, *165*, 289−316.
(29) You, Y.; Renbaum-Wolff, L.; Bertram, A. K. Liquid-Liquid Phase Separation in Particles Containing Organics Mixed with Ammonium Sulfate, Ammonium Bisulfate, Ammonium Nitrate or Sodium Chloride. *Atmos. Chem. Phys.* **2013**, *13*, 11723−11734.
(30) You, Y.; Renbaum-Wolff, L.; Carreras-Sospedra, M.; Hanna, S. J.; Hiranuma, N.; Kamal, S.; Smith, M. L.; Zhang, X.; Weber, R. J.; Shilling, J. E.; Dabdub, D. Images Reveal that Atmospheric Particles can Undergo Liquid-Liquid Phase Separations. *Proc. Natl. Acad. Sci. U.S.A.* **2012**, *109*, 13188−13193.
(31) Pöhlker, C.; Wiedemann, K. T.; Sinha, B.; Shiraiwa, M.; Gunthe, S. S.; Smith, M.; Su, H.; Artaxo, P.; Chen, Q.; Chen, Y. F.; Elbert, W.; Gilles, M. K.; Kilcoyne, A. L. D.; Moffet, R. C.; Weigand, M.; Martin, S. T.; Pöschl, U.; Andreae, M. O. Biogenic Potassium Salt Particles as Seeds for Secondary Organic Aerosol in the Amazon. *Science* **2012**, *337*, 1075−1078.
(32) Reid, J. P.; Dennis-Smither, B. J.; Kwamena, N.-O.; Miles, R. E. H.; Hanford, K. L.; Homer, C. J. The Morphology of Aerosol Particles Consisting of Hydrophobic and Hydrophilic Phases: Hydrocarbons, Alcohols and Fatty Acids as the Hydrophobic Component. *Phys. Chem. Chem. Phys.* **2011**, *13*, 15559−15572.
(33) Kwamena, N.-O.; Buajarern, J.; Reid, J. P. Equilibrium Morphology of Mixed Organic/Inorganic/Aqueous Aerosol Droplets: Investigating the Effect of Relative Humidity and Surfactants. *J. Phys. Chem. A* **2010**, *114*, 5787−5796.
(34) Buajarern, J.; Mitchem, L.; Reid, J. P. Characterizing Multiphase Organic/Inorganic/Aqueous Aerosol Droplets. *J. Phys. Chem. A* **2007**, *111*, 9054−9061.
(35) Buajarern, J.; Mitchem, L.; Reid, J. P. Characterizing the Formation of Organic Layers on the Surface of Inorganic/Aqueous Aerosols by Raman Spectroscopy. *J. Phys. Chem. A* **2007**, *111*, 11852−11859.
(36) Topping, D.; Barley, M.; McFiggans, G. Including Phase Separation in a Unified Model to Calculate Partitioning of Vapours to Mixed Inorganic−Organic Aerosol Particles. *Faraday Discuss.* **2013**, *165*, 273−288.
(37) Badger, C. L.; Griffiths, P. T.; George, I.; Abbatt, J. P. D.; Cox, R. A. Reactive Uptake of N_2O_5 by Aerosol Particles Containing Mixtures of Humic Acid and Ammonium Sulfate. *J. Phys. Chem. A* **2006**, *110*, 6986−6994.
(38) Gaston, C. J.; Thornton, J. A.; Ng, N. L. Reactive Uptake of N_2O_5 to Internally Mixed Inorganic and Organic Particles: the Role of Organic Carbon Oxidation State and Inferred Organic Phase Separations. *Atmos. Chem. Phys.* **2014**, *14*, 5693−5707.
(39) Schill, G. P.; Tolbert, M. A. Heterogeneous Ice Nucleation on Phase-Separated Organic-Sulfate Particles: Effect of Liquid vs. Glassy Coatings. *Atmos. Chem. Phys.* **2013**, *13*, 4681−4695.
(40) Davies, J. F.; Miles, R. E. H.; Haddrell, A. E.; Reid, J. P. Influence of Organic Films on the Evaporation and Condensation of Water in Aerosol. *Proc. Natl. Acad. Sci. U.S.A.* **2013**, *110*, 8807−8812.
(41) Ciobanu, V. G.; Marcolli, C.; Krieger, U. K.; Weers, U.; Peter, T. Liquid-Liquid Phase Separation in Mixed Organic/Inorganic Aerosol Particles. *J. Phys. Chem. A* **2009**, *113*, 10966−10978.
(42) Mitchem, L.; Buajarern, J.; Ward, A. D.; Reid, J. P. A Strategy for Characterizing the Mixing State of Immiscible Aerosol Components and the Formation of Multiphase Aerosol Particles Through Coagulation. *J. Phys. Chem. B* **2006**, *110*, 13700−13703.
(43) Buajarern, J.; Mitchem, L.; Reid, J. P. Manipulation and characterization of aqueous sodium dodecyl sulfate/sodium chloride aerosol particles. *J. Phys. Chem. A* **2007**, *111*, 13038−13045.
(44) About the AIOMFAC model. http://www.aiomfac.caltech.edu/about.html#references.
(45) Zuend, A. McGill University, Montreal, Quebec, CA. Personal communication, 2014.
(46) Walker, J. S.; Wills, J. B.; Reid, J. P.; Wang, L. Y.; Topping, D. O.; Butler, J. R.; Zhang, Y. H. A Direct Comparison of the Hygroscopic Properties of Ammonium Sulphate and Sodium Chloride Aerosol at Relative Humidities Approaching Saturation. *J. Phys. Chem. A* **2010**, *114*, 12682−12691.
(47) Wills, J. B.; Knox, K. J.; Reid, J. P. Optical Control and Characterisation of Aerosol. *Chem. Phys. Lett.* **2009**, *481*, 153−165.
(48) Mitchem, L.; Reid, J. P. Optical Manipulation and Characterisation of Aerosol Particles Using a Single-Beam Gradient Force Optical Trap. *Chem. Soc. Rev.* **2008**, *37*, 756−769.
(49) Preston, T. C.; Reid, J. P. Accurate and Efficient Determination of the Radius, Refractive Index and Dispersion of a Weakly Absorbing Spherical Particle Using Whispering Gallery Modes. *J. Opt. Soc. Am. B* **2013**, *30*, 2113−2122.
(50) Miles, R. E. H.; Walker, J. S.; Burnham, D. R.; Reid, J. P. Retrieval of the Complex Refractive Index of Aerosol Droplets from Optical Tweezers Measurements. *Phys. Chem. Chem. Phys.* **2012**, *14*, 3037−3047.
(51) Aden, A. L.; Kerker, M. Scattering of Electromagnetic Waves from Two Concentric Spheres. *J. Appl. Phys.* **1951**, *22*, 1242−1246.

DOI: 10.1021/acs.jpca.5b01658
J. Phys. Chem. A 2015, 119, 4177−4190

(52) Laurain, A. M. C.; Reid, J. P. Characterizing Internally Mixed Insoluble Organic Inclusions in Aqueous Aerosol Droplets and Their Influence on Light Absorption. *J. Phys. Chem. A* **2009**, *113*, 7039–7047.

DOI: 10.1021/acs.jpca.5b01658
J. Phys. Chem. A 2015, 119, 4177–4190